Title

Spin-orbit torque-driven skyrmion dynamics revealed by time-resolved X-ray microscopy

Authors

Woo, Seonghoon
Song, Kyung Mee
Han, Hee-Sung
et al.

Peer reviewed

Spin-orbit torque-driven skyrmion dynamics revealed by time-resolved X-ray microscopy

Authors: Seonghoon Woo,[1†*] Kyung Mee Song,[1,2†] Hee-Sung Han,[3] Min-Seung Jung,[4] Mi-Young Im,[4,5] Ki-Suk Lee,[3] Kun Soo Song,[1] Peter Fischer,[6,7] Jung-Il Hong,[4*] Jun Woo Choi,[1,8] Byoung-Chul Min,[1,8] Hyun Cheol Koo,[1,9] and Joonyeon Chang[1,8]

Affiliations:

[1]Center for Spintronics, Korea Institute of Science and Technology, Seoul 02792, Korea

[2]Department of Physics, Sookmyung Women's University, Seoul 04130, Korea

[3]School of Materials Science and Engineering, Ulsan National Institute of Science and Technology, Ulsan 44919, Korea

[4]Department of Emerging Materials, Research Center for Emerging Materials, DGIST, Daegu 42988, Korea

[5]Center for X-ray Optics, Lawrence Berkeley National Laboratory, Berkeley, California, 94720, USA

[6]Materials Sciences Division, Lawrence Berkeley National Laboratory, Berkeley, California, 94720, USA

[7]Department of Physics, University of California, Santa Cruz, California 94056, USA

[8]Department of Nanomaterials Science and Engineering, Korea University of Science and Technology, Daejeon 34113, Korea

[9]KU-KIST Graduate School of Converging Science and Technology, Korea University, Seoul 02792, Korea

[†] These authors equally contributed to this work

*Correspondence to: shwoo_@kist.re.kr, jihong@dgist.ac.kr

Magnetic skyrmions are topologically-protected spin textures with attractive properties suitable for high-density and low-power spintronic device applications. Much effort has been dedicated to understanding the dynamical behaviors of the magnetic skyrmions. However, experimental observation of the ultrafast dynamics of this chiral magnetic texture in real space, which is the hallmark of its quasiparticle nature, has so far remained elusive. Here, we report nanosecond-dynamics of a 100 nm-size magnetic skyrmion during a current pulse application, using a time-resolved pump-probe soft X-ray imaging technique. We demonstrate that distinct dynamic excitation states of magnetic skyrmions, triggered by current-induced spin-orbit torques, can be reliably tuned by changing the magnitude of spin orbit torques. Our findings show that the dynamics of magnetic skyrmions can be controlled by the spin-orbit torque on the nanosecond time scale, which points to exciting opportunities for ultrafast and novel skyrmionic applications in the future.

Most magnetic materials show collinear magnetic ordering due to the large exchange interaction between neighbouring magnetic moments. However, provided the Dzyaloshinskii-Moriya interaction (DMI)[1,2] is strong enough to overcome the exchange interaction, magnetic spins tend to align in non-collinear fashion with fixed homochirality. Most notably, in structures where the broken inversion symmetry leads to sufficiently large DMI, non-trivial small cylindrical swirling spin structures, called chiral magnetic skyrmions can be energetically stable[3–16]. Unlike magnetic bubble domains[17,18], chiral magnetic skyrmions[3–16] exhibit fascinating behaviors such as lattice formation[4,6,7,14], emergent electrodynamics[19] and current-driven displacement at low current densities[9–11]. Recently, micromagnetic simulations have predicted[11] and experiments confirmed[13–16] that chiral magnetic skyrmions can be created at room temperature in robust metallic thin film heterostructures such as Ta/CoFeB/TaO$_x$[13], Pt/Co/Ta, Pt/CoFeB/MgO[14] Pt/Co/Ir[15], and Pt/Co/MgO[16] in the presence of a strong interfacial DMI. In such structures, current-pulse induced skyrmion displacement was achieved by harnessing spin-orbit torques (SOTs)[20–22] from non-magnetic heavy metals such as Ta and Pt. The experimental realization of the current induced skyrmion motion is particularly important for the development of skyrmion based memory devices[11,23]. However, earlier studies were limited to the static position imaging of magnetic skyrmions before and after the current pulses. Direct observation of nanosecond dynamics of sub-100 nm sized skyrmions in real space *during* the current pulse applications is required, not only for a better physical understanding of current driven skyrmion motion, but also for the exploration of new dynamical phases[12] of skyrmions. This has remained elusive so far, due to the high frequency and high spatial resolution measurement regimes required for such observations that are not easily accessible in experiments.

Here we report direct observation of chiral magnetic skyrmion dynamics induced by SOTs in a transition metal ferromagnet multilayer at room temperature. By utilizing a stroboscopic pump-probe technique in a full-field magnetic transmission soft X-ray microscope (MTXM), we image the development of time-dependent transformation of chiral magnetic skyrmions while a nanosecond current pulse is being applied. First, we demonstrate the generation of skyrmions at zero magnetic field by applying bipolar electric current pulses. We then observe that the skyrmions show two distinct dynamic behaviours, the breathing and the translational excitation behaviours, depending on the magnitude of SOTs, which is directly proportional to the current pulse amplitude.

MTXM observation of domain textures and DMI constant measurement

The multilayer structure in our study consists of [Pt (3 nm) / $Co_4Fe_4B_2$ (0.8 nm) / MgO (1.5 nm)]$_{20}$ (hereafter Pt/CoFeB/MgO) with perpendicular magnetic anisotropy (PMA). Figure 1a shows the out-of-plane hysteresis loop measured by vibrating sample magnetometry (VSM) of the Pt/CoFeB/MgO multilayer, while the inset shows that of the Pt/CoFeB/MgO unit layer. Vanishing remnant magnetization in the multilayer structure is due to the formation of multi-domain states in the absence of magnetic field, which results from the strong de-magnetizing field and the small domain wall surface energy of large DMI structures (See Supplementary Information S1 for details). This is confirmed by the MTXM magnetic domain images in Fig. 1b, where dark and bright contrast corresponds to down and up domains, respectively. Micromagnetic simulations show that the magnetic texture in each layer is coupled magneto-statically across the entire stack (See Supplementary Information S2), thus the magnetic contrast is significantly enhanced in the transmission X-ray measurement. Since the prerequisite for the formation of the chiral Néel DWs is a large DMI, we first determine the DMI constant

analytically by measuring the field-dependent domain size variation for both up- and down-oriented domains from the sequence of MTXM images in Fig. 1b (See Supplementary Information S1 for details). Alternatively the DMI constant in the Pt/CoFeB/MgO structure was quantified by field-driven domain expansion experiments and spin-Hall effect efficiency measurements (See Supplementary Information S3 and S4 for details). Using these measurements, we found that the magnitude of DMI is approximately $|D|$ = 1.68 mJ/m^2, which is in good agreement with reported values for Pt/CoFeB interface[14,24] and significantly larger than the critical value required to stabilize Néel DWs[25], $|D_c| \approx (2\ln 2)\mu_0 M_s^2 t / \pi^2 \approx$ 0.11 mJ/m^2.

Moreover, by analyzing the asymmetry of the field driven DW expansion (Supplementary Information S3), we find that the Pt/CoFeB/MgO structures have homochiral left-handed Néel walls stabilized by DMI. This is shown schematically in Fig. 1c.

Electrical generation of magnetic skyrmions at zero magnetic field

To study electric current driven magnetic domain dynamics in these systems, the magnetic multilayer films were patterned into 2 µm-wide magnetic strips, with 5 µm-wide and 100 nm-thick Au electrodes, used to inject electric current pulses, deposited on the top of the strips. Figure 2a shows the schematics of the electrical set-up used for the current-induced measurements. We first demonstrate the electrical generation of magnetic skyrmions in the absence of magnetic field using static X-ray measurements. MTXM magnetic domain images acquired at zero field are shown in Fig. 2b. Before the pulse injection, two representative areas (left-panel images in Fig. 2b (i) and (ii)) of the magnetic strip showed the characteristic labyrinth

multi-domain state. 20 ns-long bipolar voltage pulses with an amplitude of V_a=2.5V (where

V_{pp}=5V), which corresponds to the current density of ~ $|j_a| = 1.6 \times 10^{11}$ A/m^2, were then applied to

the strip. The pulses were applied at a repetition rate of f = 3.33 MHz for a time span of five

seconds. The right-panel images in Fig. 2b (i) and (ii) show that the labyrinth domains with

chiral domain walls are completely transformed into multiple circular domains after the pulse

applications, which we later confirm to indeed be chiral magnetic skyrmions from the

observation of their current driven dynamics. In this system, chiral domain wall motion is

induced by the SOT at the Pt/CoFeB interface which switches polarity with the current pulse

direction[22,24]. Then bipolar pulses are expected to excite the system by driving the domain walls

back and forth. Such excitations could provide enough activation energy for the system to find

the ground state magnetic domains without changing the net magnetization. Therefore, we

believe that the most stable state of the Pt/CoFeB/MgO multilayer system, which is the multiple

skyrmionic state, can be achieved with a bipolar pulse-induced excitation. In fact, we can

compare our calculated DMI constant, $|D|$ = 1.68 mJ/m^2, with the threshold DMI value,

$|D_{th}| = 2.26$ mJ/m^2, for the spontaneous skyrmion generation by leading to negative domain wall

energy, where $\sigma_{DW} < 0$. It is clear that our material system has relatively low DMI value, which

is not enough to drive the system into multiple skyrmions or skyrmion lattice in the absence of

external excitation. However, as the DMI value is still significantly larger than the critical value

6

required stabilizing Néel DWs, $|D_{th}| = 0.11$ mJ/m^2, once the system reaches to a state with multiple skyrmions, the multi-skyrmion state remains far more stable. Note that skyrmion distribution observed in Fig. 2b show rather random size distribution and the lack of lattice structure, which can also be explained by the DMI value lower than the threshold. This is supported by the micromagnetic simulation study in Refs. [12,26] that shows current injection can provide sufficient energy to induce strong topological fluctuations to switch the system into a more stable state. Specifically, Ref. 25 described the evolution of a single skyrmion state (net topological number, Q=1) from ferromagnetic state (Q=0) in a confined magnetic disk structure by nanoseconds bipolar-pulse injections with micromagnetic simulations, and showed that current pulse polarity-changes in nanoseconds time scale can induce the abrupt change of topological number, resulting in the emergence of topological state, *skyrmions*, after the pulse. A similar experimental observation was also reported in Ref. [14] in which skyrmions were stabilized after applying bipolar *magnetic* field oscillations. We also confirmed that the magnetic properties of our film are preserved even after the pulse-induced skyrmion generation as discussed in Supplementary Information S5.

Time-resolved X-ray microscopy measurement on magnetic skyrmions

Finally, we demonstrate current-driven dynamics of skyrmions utilizing the SOTs from the spin Hall effect (SHE). It has been predicted that skyrmions may be nucleated and stabilized dynamically by the combination of vertical spin current injection and the corresponding spin transfer torque, in material systems with relatively large DMI[12]. Experimentally, this spin torque can be achieved by SOTs via SHE[22] from an in-plane current flowing along a non-magnetic heavy metal layer such as Pt. The spin Hall angle in our Pt/CoFeB/MgO structure is measured to be $\theta_{SH} = +0.08$, which is determined by the current-induced hysteresis loop shift experiments[24]

(See Supplementary Information S4 for details). The large SOT originating from this SHE could efficiently actuate skyrmion motion in our magnetic track[11,13,14]. To study the skyrmion dynamics, time-resolved pump-probe MTXM experiments using the 2-bunch mode at Advanced Light Source (ALS) were performed (See Methods for details). Figure 3a shows the schematics of the device configuration and measurement scheme with an X-ray image of the device enclosed. Figure 3a also shows an MTXM image of a single isolated skyrmion in this device. The isolated skyrmion state, generated by applying an external magnetic field $B_z = +12.5$ mT to the multiple skyrmion state, was chosen for the dynamic measurements to avoid possible skyrmion-skyrmion interactions. The actual temporal evolution of the bipolar current pulse is plotted in Fig. 3b, showing a rise/fall time of ~2.5 ns and an effective pulse width of roughly ~5 ns for each up/down pulse. Small reflected pulses are also observed due to the impedance mismatch, where R_{sample}~100 Ohms. For the time-resolved measurements, the amplitude of the bipolar current pulse was varied between V_a = 1.5 V and V_a = 2.5 V, which correspond to the current density of $|j_a| = 9.8 \times 10^{10}$ A/m² and $|j_a| = 1.6 \times 10^{11}$ A/m², respectively. When, we first applied a low voltage of V_a=1.5V to the sample, there was no observable change in shape as well as in position of the skyrmion (see Supplementary Information S6 for details). Then the pulse amplitude was increased. The dynamic behaviors of skyrmions upon the applications of pulses with V_a =2V and 2.5V are shown in Figure 3c and 3e, respectively. The coloured circles in this plot indicate the time delay, which is also shown in Fig. 3b. When the pulse amplitude V_a=2V (Fig. 3c), a strong breathing-like excitation behavior of the skyrmion is observed. The center position of the skyrmion remains stationary at all times, while the skyrmion diameter changed by roughly a factor of two: from 190 nm at t=6 ns (positive pulse) to 85 nm at t=16 ns (negative pulse). The

size variation was clearly noticeable due to the high spatial-resolution of the X-ray microcopy with the limit of ~25nm due to the optical instruments. (Details about the measurement of the skyrmion size are explained in Supplementary Information S7.) This observation of magnetic skyrmion breathing-like behaviour offers the first experimental demonstration of SOT-induced nanosecond dynamics for magnetic skyrmion. Fig. 3d simultaneously shows time-dependent progression of skyrmion diameter and current pulse application, revealing the time-dependent skyrmion response to the voltage pulse. It is obvious that the skyrmion expands by about a factor of 2 under a positive current pulse while it only shrinks ~20% under a negative pulse. This *asymmetric* breathing-like excitation behaviour can be understood using a 'SOT+Oersted field model', which is described later in detail in Fig. 4. Moreover, it should be noted that negligible time delay exists (less than a nanosecond measured from graph); the skyrmion size is largest when the pulse position is at its highest amplitude. This may indicate that the chiral magnetic skyrmion in our structure has small inertia, whereas the inertia of non-chiral bubbles reported in Ref. [27] are rather large. As we further increase the pulse amplitude (Fig. 3e), a local translation of magnetic skyrmion is observed with the maximum displacement of ~84 nm, in addition to the skyrmion size variation. In Fig. 3f, we plot the time-dependent skyrmion displacement and pulse progression simultaneously, showing that a skyrmion moves upward with the velocity of ~10 m/s, which has only been shown statically in earlier studies[13,14]. It moves back to its original position during the negative cycle of the bipolar pulse. Therefore, temporal images in Fig. 3e effectively show the time-dependent displacement of a skyrmion during its current induced translation. Fig. 3f can also be used to analyze inertial motion of a magnetic skyrmion, Fig. 3f can also be used to analyze inertial motion of a magnetic skyrmion. More thorough discussion on the inertial effect of skyrmions is described in the last part of this article. We also find that the

skyrmion moves against the electron flow direction in our structure (schematically shown in Fig. 3e), as expected from the SOT-driven transport characteristics of left-handed Néel skyrmions[14,28]. The velocity and threshold for translational mode can be compared with previous experiment on static displacement of skyrmions in a similar Pt/CoFeB/MgO multilayer structure in Ref. 14,

where the rough threshold for skyrmion motion $|j_c| = 1.5 \times 10^{11}$ A/m^2 falls between the current

densities applied in our study for Fig. 3c, $|j_a| = 1.3 \times 10^{11}$ A/m^2, and Fig. 3e, $|j_a| = 1.6 \times 10^{11}$ A/m^2;

the velocity at similar current density also resembles such. From these experimental observations, we first speculate that SOTs could induce two different dynamical behaviours: the breathing-like and the translational excitation behaviors. Simply changing the external current pulse amplitude can tune between the modes. The full movie of the skyrmion motion can be found in Supplementary Movies 1-3.

Micromagnetic simulation on skyrmion dynamics and comparison with experimental observation

To support our experimental observation, we performed micromagnetic simulations shown in Figure 4 to further investigate the observed skyrmion dynamics (see Methods for simulation details). A larger magnetic field of B_z=+48 mT was applied for the simulation, compared to B_z=+12.5 mT used in experiments, to achieve a skyrmion size compatible with experiments and also avoid possible inter-skyrmion interaction in a given mesh-dimension with a periodic boundary condition. Fig. 4a first shows a skyrmion stabilized at its equilibrium state in the presence of external magnetic field, and Fig. 4b indicates the pulse profile used for the simulation, exhibiting a slightly different pulse shape from the one used in experiment (shown in

Fig. 3b); in the computational approach, there is no reflected pulse because perfect impedance matching is assumed. First, to understand breathing-like excitation behaviours shown in Fig. 3c, we analyze time-dependent skyrmion diameter variation during the pulse application with three different models. The bipolar pulse amplitudes of V_{Low} (= 2 V) and V_{High} (= 6 V) are used. For V_{High}, the simulation result presented in Fig. 4c(i) first reveals that the application of SOTs, which induces strong topological fluctuation, only *increases* the skyrmion diameter regardless of pulse direction. Thus, if our experimental observation is only driven by SOTs, we should have observed skyrmion breathing-like behaviour with a frequency, ~0.2GHz, which is twice the pulse frequency. However, as observed in Fig. 3c and 3d, the breathing-like behaviour has the same frequency with the bipolar pulse, ~0.1GHz, and the breathing amplitude is significantly stronger. This discrepancy can be compensated when we considered the Oersted field effect, which varied in linear proportion with current pulse. Note that our skyrmion is located near an Au electrode, as shown in the inset micrograph of Fig. 3a, thus, a finite Oersted field effect can be reasonably expected. Fig. 4c(ii) shows the skyrmion size variation when we *only* consider the time-varying Oersted field generated by current pulses. A *symmetric* skyrmion breathing-like behaviour, driven by a bipolar Oersted field of 2Oe per 1V pulse amplitude, is observed in Fig. 4c(ii). This model still fails to match the experimentally observed *asymmetric* expansion shown in Fig. 3c and 3d. However, as we combine these two effects simultaneously as shown in Fig. 4c(iii), strong *asymmetric* breathing-like behaviour is expected, and surprisingly, our experimental observation presented in Fig. 3c is reproduced qualitatively, as shown in Fig. 4d. Therefore, the suggested SOT+Oersted field model can successfully explain the experimentally observed skyrmion breathing-like behaviour. It should be noted that for V_{Low}, the SOT is too small (Fig. 4c(i)) to induce skyrmion size variation so that only a small symmetric Oersted field driven

11

motion is expected (Fig. 4c(iii)). The small amplitude of this symmetric motion ~5nm in Fig. 4c(iii), cannot be observed experimentally (Supplementary Information S6) due to the limiting MTXM spatial resolution. It should also be noted that the observed breathing-like behaviour is not the internal skyrmion *breathing mode,* which happens when an oscillating magnetic field $h_z(t)$ matches the specific resonant criteria of surrounding Néel domain walls in the frequency regime of at least a few GHz as studied in Ref. [29]. Nevertheless, through the analysis shown in Fig. 4, we clearly show that the application of nanosecond current pulses induce a breathing-like skyrmion behaviour. In particular the simulation results in 4c(i) suggest that SOT-only can still induce the size variation via strong topological fluctuation. In this case, an applied pulse would enlarge the skyrmion regardless of the pulse direction, and as soon as the pulse turns off, the skyrmion returns back to its equilibrium size. The SOT-driven breathing behaviour can be further maximized by using heavy metal layers with large spin-Hall effect such as W (spin Hall angle θ_{SH}=0.3)[30] or facet-engineered IrMn$_3$ (θ_{SH}=0.35)[31], since the SOT-driven size variation is linearly proportional to the spin Hall effect (θ_{SH}=0.08 in our system). , Furthermore, we expect the pulse-length can easily tune the breathing frequency. Therefore, we believe our result provides very important implicadtion that, in an engineered material with strong spin orbit effect, we can realize a strong SOT-driven skyrmion breathing-like dynamics by simply turning on and off the external current pulses in the nanosecond time scale.

We then applied the same models for analysing skyrmion travel distance as a function of time, as shown in Fig. 4e and 4f. Fig. 4e clearly show that the SOT can induce translational motion of the skyrmions, while the Oersted field cannot. When the experimental result (Fig. 3f) and computed model (Fig. 4f) are compared, the time-dependent travel distances agree qualitatively. However, unlike the experiments in which the translational skyrmion mode was

only observed for current pulses larger than the threshold, in simulations, the pulse-injection always triggers a simultaneous skyrmion displacement as shown in Fig. 4e. This difference can be explained by material deficiencies, such as non-uniform DMI, which were not considered in simulations. In non-epitaxial sputtered films, the DMI constant can be non-uniform over a single film, resulting in finite pinning threshold that traps skyrmion and requires large current to actuate its motion[14]. Therefore, it is likely that there exists sizable DMI variation over the actual sample, which effectively provides pinning threshold, so that only radial size variation was observed in Fig. 3c without its core-displacement. Once the excitation energy overcomes the threshold with larger current pulses, the translational motion is actuated. Considering the imperfections always existing in real magnetic films, we believe our experimental observations provide a practical way to induce and tune between distinct skyrmion dynamic states simply by changing the SOTs. However, we also show that our observed skyrmion was not locating at a strong local pinning site, which deforms the surrounding domain walls thus enabling easy skyrmion destruction with external fields or pulses. We discuss the effect of the strong pinning via micromagnetic simulations in Supplementary Information S8. Finally, it should be noted that, while the experimental and computational results of the skyrmion size variation and travel distance agree qualitatively, there still exists *quantitative* discrepancy again possibly due to material deficiencies, such as non-perfect interfaces, errors in estimating the Oersted field, errors in determining the spin Hall angle, etc. Even if we regret that we are not able to clearly elucidate the reasoning on the difference, however, we believe the additional investigations can be additionally done in the following work, which goes beyond the scope of this paper.

Inertial effect of magnetic skyrmion motion and its deformation

The time-dependent skyrmion displacement, shown in 4e, could be used for studying the *inertial* motion of magnetic skyrmions. Based on the successful agreement between experiment and simulation (Fig. 4f), the computational data in Fig. 4f is utilized for more in-depth analysis. We first plot the travel distance and voltage pulse as a function of time in Fig. 5a, and also plot its derivative: *velocity* and voltage pulse in Fig. 5b. In spin textures such as skyrmions and domain walls with massless-particle approximation, as can be derived from the Thiele's equation[32], the velocity is linearly proportional to external forces. Thus, if there exists an *inertial* effect, we should be able to observe a finite skyrmion displacement (implying finite velocity) even in the absence of external force, which is the current pulse in the present case. However, as

we plot the velocity ($v = \dfrac{dD}{dt}$) as a function of time in Fig. 5b, it is evident that the velocity and

force curves are perfectly matching, implying that there is no observable (up to the spatial resolution limit ~25nm of the MTXM) inertial effect on the skyrmion motion in our system. The agreement between the computational model and the time-dependent displacement of experimentally observed skyrmions (Fig. 4f) further validates our conclusion on *inertial motion* even for the real case. This observation is reasonable as the concept of "*inertial*" is a completely misconception in a magnetic system only described by the LLG equation. According to the LLG equation as a consequence of the first order derivative in time, each spin in a texture such as a domain wall or a skyrmion should simultaneously obtain their velocity from any external forces such as magnetic field and/or electrical current, and this is clearly shown in Ref. [[33]]

However, it should be pointed out that our observation disagrees with the recent experimental observation of skyrmion bubble dynamics, showing the presence of strong inertia

14

and the areal mass being as large as 2.0×10^{-7}kg m^{-2}.[27] We believe the difference originates from the fact that the inertial motion of a skyrmion can be enhanced in a confined geometry. In a situation where spin dynamics can be fully reproduced using Landau-Lifshitiz-Gilbert (LLG) equation, inertial behaviour cannot appear as we stated above. Indeed, it has been shown that the dynamics of vortices in thin ferromagnetic films can be successfully reproduced without introducing the concept of inertia, where the vortices have a finite topological invariant known as the skyrmion charge $q = (1/4\pi)\int dx dy \mathrm{m} \cdot (\partial_x \mathrm{m} \times \partial_y \mathrm{m})$; where vortexes have $q = \pm 1/2$.[34,35] However, in situations where the LLG equation fails so that the collective coordinate should be implemented, the concept of inertia can be introduced to correctly reproduce the observed spin dynamics such as skyrmion bubble gyration in a confined geometry.[27,36] In our case where a skyrmion locates in a quasi-infinite thin film, thus, its dynamic behaviour such as translation or breathing-like motion can be simply reproduced without implementing collective coordinate model. During the submission of this work, Litzius *et al*.[37] reported the observation of skyrmion Hall effect in Pt/CoFeB/MgO multilayers using time-resolved X-ray microscopy method, which works in very similar fashion with MTXM used in this work.

In summary, we investigated the ultrafast dynamics of a magnetic skyrmion in the nanosecond time scale using time-resolved X-ray microscopy in order to better understand the physical origin behind the current induced skyrmionic motion. We demonstrated electrical generation of magnetic skyrmions in the absence of magnetic field by using bipolar pulses. By changing the magnitude of SHE-induced SOTs with the current amplitude, we have revealed the manipulation of skyrmion dynamics between the breathing-like and the translational excitation behaviors. Our observations offer an efficient method to manipulate chiral magnetic skyrmions both statically and dynamically, which are an essential requirement for the development of

15

broadband low power and high density skyrmionic devices. Therefore, our observation indeed opens the door to versatile and novel skyrmionic applications.

Methods

The [Pt(3nm)/CoFeB(0.8nm)/MgO(1.5nm)]$_{20}$ films were grown on a 100nm-thick SiN substrate by dc magnetron sputter deposition at room temperature under 3 mTorr Ar for Pt, 1 mTorr Ar for CoFeB and 4 mTorr Ar for MgO, with a background pressure lower than ~$3\text{x}10^{-8}$ Torr. Ta seed, t_{seed}=3nm, and capping, $t_{capping}$=2nm, layers were deposited for better adhesion to SiN substrate and protection from atmospheric conditions, respectively. The thin film samples then patterned using electron beam lithography and ion-milling techniques. Nominally identical films were grown on SiOx/Si substrates for vibrating sample magnetometry (VSM) measurements. The VSM measurements yielded an anisotropy field of $\mu_0 H_k$ = 0.7 T, and a saturation magnetization of M_s = $9\text{x}10^5$ A/m. The current contacts in Fig. 2 and Fig. 3 consisted

of Ti (5 nm) / Au (100 nm), which was deposited using the same dc magnetron sputtering. The contacts were also patterned using electron beam lithography and lift-off. For the current-density calculations used in Fig. 3 and maintext, we only considered Pt and CoFeB layers while excluding Ta layers, which is expected to be high resistivity   -phase.

All images in the main text and supplementary materials were acquired using full-field MTXM performed at the XM-1 beamline 6.1.2 at the Advanced Light Source (ALS) in Berkeley, California. The device used for experiments was 2 µm-wide with electrical resistance of ~ 100 Ohms between two Au contacts. Pulse current densities above ~2×10^{11} A/m^2 led to the damage of the Au contact, which eventually limited the maximum current applied in Fig. 3. In time-resolved 2-bunch experiments, where X-rays are injected at 300 ns intervals (injection frequency of 3.33 MHz), the stroboscopic pump-probe technique of MTXM restricts the imaging to fully reproducible magnetic events by synchronizing the incoming X-ray photon flashes (probe) and injecting current pulses (pump). The time evolution of the dynamics was recorded by varying the delay times between the photon flashes and the excitation pulses. Due to the low intensity for a single X-ray pulse, about 10^8-10^9 pump-probe events are required to obtain a single magnetic image shown in Fig. 3, which corresponds to an accumulation time per image of a few tens of seconds. To ensure that all acquired images in Fig. 3 indicate the exactly same area of our ferromagnetic wire, we have performed the image-displacement correction by aligning Au contact boundary near our skyrmion across all acquired images using computer software. This allows us to align all images to the same position within error of a pixel size, ~25nm.

Micromagnetic simulations were performed using open-source MuMax[3] and it solved Landau-Lifshitiz-Gilbert (LLG) equation: $\partial \mathbf{m}/\partial t = -\gamma_0 \mathbf{m} \times \mathbf{H_{eff}} + \alpha \mathbf{m} \times \partial \mathbf{m}/\partial \square - \gamma_0 \mathbf{m} \times (\mathbf{m} \times \mathbf{H_{SH}} \ \hat{y})$[38,39] where $\mathbf{H_{SH}} = \mu_B \theta_{SH} j_a / \gamma_0 e M_s t_z$ with normalized local magnetization vector $\mathbf{m}$, the gyromagnetic

17

ratio γ_0, the effective field $\mathbf{H_{eff}}$, damping constant α, Bohr magneton μ_B, spin Hall angle θ_{SH}, the current density j_a which flows in the sample along x-direction, saturation magnetization M_s, charge of electron e, and thickness of ferromagnetic layer t_z. To model multilayer film [Pt (3 nm) / CoFeB (0.8 nm) / MgO (1.5 nm)]$_{20}$, 20 ferromagnetic layers of $600 \times 600 \times 0.8$ nm^3 is employed with the cell size of $2 \times 2 \times 0.8$ nm^3, and the distance between each ferromagnetic layers was kept to be 4.8 nm to replicate Pt and MgO layers in experiments. To ignore the effect of the lateral sample edges, we adopt a periodic boundary condition along in-plane direction. Material parameters used are an exchange stiffness $A_{ex} = 1.4 \times 10^{-11}$ J/m, saturation magnetization $M_s = 9 \times 10^5$ A/m^3, Dzyaloshinskii Moriya constant $D = 1.4$ mJ/m^2, uniaxial anisotropy constant $K_u = 7.79 \times 10^5$ A/m^3, damping constant $\alpha = 0.5$, and spin Hall angle $\theta_{SH} = 0.1$. The current density $j_a = 5.48 \times 10^{10}$ A/m^2 corresponds to $V_a = 1$ V in SOT-related simulations.

References.

1. Dzyaloshinsky, I. A thermodynamic theory of 'weak' ferromagnetism of antiferromagnetics. *J. Phys. Chem. Solids* **4,** 241–255 (1958).

2. Moriya, T. Anisotropic Superexchange Interaction and Weak Ferromagnetism. *Phys. Rev.* **120,** 91–98 (1960).

3. Rößler, U. K., Bogdanov, A. N. & Pfleiderer, C. Spontaneous skyrmion ground states in magnetic metals. *Nature* **442,** 797–801 (2006).

4. Mühlbauer, S. *et al.* Skyrmion Lattice in a Chiral Magnet. *Science* **323,** 915–919 (2009).

5. Yu, X. Z. *et al.* Real-space observation of a two-dimensional skyrmion crystal. *Nature* **465,** 901–904 (2010).

6. Münzer, W. *et al.* Skyrmion lattice in the doped semiconductor ${\text{Fe}}_{1$-${}x} {\text{Co}}_{x}\text{Si}$. *Phys. Rev. B* **81,** 041203 (2010).

7. Heinze, S. *et al.* Spontaneous atomic-scale magnetic skyrmion lattice in two dimensions. *Nat. Phys.* **7,** 713–718 (2011).

8. Yu, X. Z. *et al.* Near room-temperature formation of a skyrmion crystal in thin-films of the helimagnet FeGe. *Nat. Mater.* **10,** 106–109 (2011).

9. Yu, X. Z. *et al.* Skyrmion flow near room temperature in an ultralow current density. *Nat. Commun.* **3,** 988 (2012).

10. Iwasaki, J., Mochizuki, M. & Nagaosa, N. Current-induced skyrmion dynamics in constricted geometries. *Nat. Nanotechnol.* **8,** 742–747 (2013).

11. Fert, A., Cros, V. & Sampaio, J. Skyrmions on the track. *Nat. Nanotechnol.* **8,** 152–156 (2013).

12. Zhou, Y. *et al.* Dynamically stabilized magnetic skyrmions. *Nat. Commun.* **6,** 8193 (2015).

13. Jiang, W. *et al.* Blowing magnetic skyrmion bubbles. *Science* aaa1442 (2015). doi:10.1126/science.aaa1442

14. Woo, S. *et al.* Observation of room-temperature magnetic skyrmions and their current-driven dynamics in ultrathin metallic ferromagnets. *Nat. Mater.* **15,** 501–506 (2016).

15. Moreau-Luchaire, C. *et al.* Additive interfacial chiral interaction in multilayers for stabilization of small individual skyrmions at room temperature. *Nat. Nanotechnol.* **11,** 444–448 (2016).

16. Boulle, O. *et al.* Room-temperature chiral magnetic skyrmions in ultrathin magnetic nanostructures. *Nat. Nanotechnol.* **11,** 449–454 (2016).

17. Malozemoff, A. P. Mobility of bubbles with small numbers of Bloch lines. *J. Appl. Phys.* **44,** 5080–5089 (1973).

18. Malozemoff, A. P. & Slonczewski, J. C. *Magnetic domain walls in bubble materials.* (Academic Press, 1979).

19. Schulz, T. *et al.* Emergent electrodynamics of skyrmions in a chiral magnet. *Nat. Phys.* **8,** 301–304 (2012).

20. Mihai Miron, I. *et al.* Current-driven spin torque induced by the Rashba effect in a ferromagnetic metal layer. *Nat. Mater.* **9,** 230–234 (2010).

21. Miron, I. M. *et al.* Perpendicular switching of a single ferromagnetic layer induced by in-plane current injection. *Nature* **476,** 189–193 (2011).

22. Liu, L. *et al.* Spin-Torque Switching with the Giant Spin Hall Effect of Tantalum. *Science* **336,** 555–558 (2012).

23. Kiselev, N. S., Bogdanov, A. N., Schäfer, R. & Rößler, U. K. Chiral skyrmions in thin magnetic films: new objects for magnetic storage technologies? *J. Phys. Appl. Phys.* **44,** 392001 (2011).

24. Pai, C.-F., Mann, M., Tan, A. J. & Beach, G. S. D. Determination of spin torque efficiencies in heterostructures with perpendicular magnetic anisotropy. *Phys. Rev. B* **93,** 144409 (2016).

25. Thiaville, A., Rohart, S., Jué, É., Cros, V. & Fert, A. Dynamics of Dzyaloshinskii domain walls in ultrathin magnetic films. *EPL Europhys. Lett.* **100,** 57002 (2012).

26. Yuan, H. Y. & Wang, X. R. Skyrmion Creation and Manipulation by Nano-Second Current Pulses. *Sci. Rep.* **6,** 22638 (2016).

27. Büttner, F. *et al.* Dynamics and inertia of skyrmionic spin structures. *Nat. Phys.* **11,** 225–228 (2015).

28. Emori, S., Bauer, U., Ahn, S.-M., Martinez, E. & Beach, G. S. D. Current-driven dynamics of chiral ferromagnetic domain walls. *Nat. Mater.* **12,** 611–616 (2013).

29. Kim, J.-V. *et al.* Breathing modes of confined skyrmions in ultrathin magnetic dots. *Phys. Rev. B* **90,** 064410 (2014).

30. Pai, C.-F. *et al.* Spin transfer torque devices utilizing the giant spin Hall effect of tungsten. *Appl. Phys. Lett.* **101,** 122404 (2012).

31. Zhang, W. *et al.* Giant facet-dependent spin-orbit torque and spin Hall conductivity in the triangular antiferromagnet IrMn3. *Sci. Adv.* **2,** e1600759 (2016).

32. Thiele, A. A. Steady-State Motion of Magnetic Domains. *Phys. Rev. Lett.* **30,** 230–233 (1973).

33. Wang, X. R., Yan, P., Lu, J. & He, C. Magnetic field driven domain-wall propagation in magnetic nanowires. *Ann. Phys.* **324,** 1815–1820 (2009).

34. Guslienko, K. Y. *et al.* Eigenfrequencies of vortex state excitations in magnetic submicron-size disks. *J. Appl. Phys.* **91,** 8037–8039 (2002).

35. Choe, S.-B. *et al.* Vortex Core-Driven Magnetization Dynamics. *Science* **304,** 420–422 (2004).

36. Moutafis, C., Komineas, S. & Bland, J. A. C. Dynamics and switching processes for magnetic bubbles in nanoelements. *Phys. Rev. B* **79,** 224429 (2009).

37. Litzius, K. *et al.* Skyrmion Hall effect revealed by direct time-resolved X-ray microscopy. *Nat. Phys.* **advance online publication,** (2016).

38. Landau, L. D. & Lifshitz, E. On the theory of the dispersion of magnetic permeability in ferromagnetic bodies. *Phys Z Sowjetunion* **8,** 101–114 (1935).

39. Gilbert, T. L. A phenomenological theory of damping in ferromagnetic materials. *IEEE Trans. Magn.* **40,** 3443–3449 (2004).

Author Contributions

S.W. designed and initiated the study. S.W. and K.M.S. fabricated devices and performed the film characterization. K.S.S. provided technical input for nano-fabrication using e-beam lithography. S.W., K.M.S., M.-S.J., M.-Y.I. and J.W.C. performed X-ray imaging experiments using MTXM with supports from J.-I.H. at the Advanced Light Source in Berkeley, California.

H.-S.H. and K.-S.L. performed micromagnetic simulations. All authors participated in the discussion and interpretion of the results. S.W. and J.W.C. drafted the manuscript and revised it with assistance from M.-Y.I., K.-S.L., P.F., J.-I.H., B.-C., H.C.K. and J.C. All authors commented on the manuscript.

Author Information

The authors declare no competing financial interests. Correspondence and requests for materials should be addressed to S.W. (shwoo_@kist.re.kr) and J.-I.H. (jihong@dgist.ac.kr)

Figure legends.

Figure 1. Structural characteristics and X-ray imaging of domain patterns. a, Out-of-plane hysteresis loop for a companion multilayer film grown on Si wafer. The magnetic moment is normalized to its saturation magnetization $M_S = 9 \times 10^5$ A/m. The inset shows both in-plane and out-of-plane hysteresis loops for a Pt/CoFeB/MgO unit layer grown on Si wafer. **b,** Series of MTXM images acquired for increasing field $B_z > 0$. Dark and light contrast corresponds to down (-z) and up (+z) –oriented magnetization directions, respectively. **c,** MTXM image acquired at B_z =25mT and the schematic of the expected chiral magnetic textures.
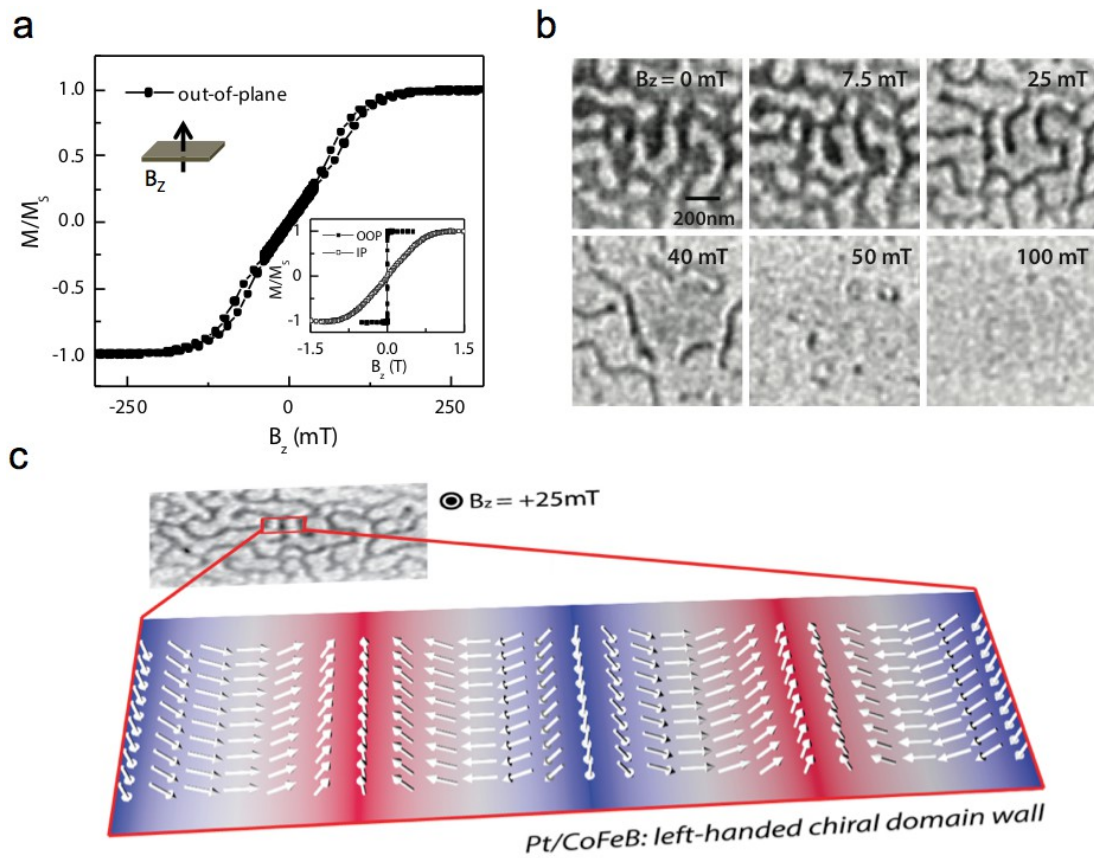
Figure 2. Electrical generation of magnetic skyrmions. a, Schematic of the electric connection for current pulse-injection experiments. The X-ray beam is injected at the frequency of 3.33 MHz (bunch spacing = 300 ns) and can be synchronized with current pulses to observe temporal evolution of magnetic textures. A source meter is connected through a bias-tee to simultaneously measure the device resistance. The SEM image of the actual device is also shown. **b,** MTXM images of the magnetic domain states showing the transformation of domain phase from labyrinth state to multiple skyrmionic state after the application of bipolar pulses at $B_z = 0$ mT. Enclosed SEM image shows two distinct areas in a magnetic wire, (i) and (ii), where the magnetic textures were separately measured. Bipolar pulse trains are injected at $f = 3.33$ MHz for 5 s. Images are taken before (left) and after (right) the current pulses.

Figure 3. Dynamic behavior of a magnetic skyrmion induced by bipolar pulse injections. a, Schematic of the Pt/CoFeB/MgO magnetic wire on the Si_3N_4 membrane with electrode contacts. The skyrmions are stabilized in the magnetic wire at B_z=12.5 mT. The inset shows an initial skyrmion used for the dynamic measurement. **b,** Pulse profile used for the dynamics measurement. There is a time delay between each bipolar pulse and the incident X-ray beam pulse, which are injected at a frequency of $f = 3.33$ MHz. The coloured circles in this plot indicate the time delay, which is also shown in following images. Magnetic skyrmion configuration at different time delays for voltage amplitudes of **c,** $V_a = 2$ V and **e,** $V_a = 2.5$ V, respectively. Black arrows are included in **e** to indicate the direction of electron flow at each time delay, and schematic drawing is also included on the right side to more clearly show the directions. Horizontal lines are drawn in **c** and **e** to more effectively show the variation of the skyrmion. **d,** Measured skyrmion size and **e,** total skyrmion travel distance as a function of pulse delay time, respectively. The actual pulse profile, shown in **b**, is also included in both plots to effectively show the response of skyrmion to time-dependent pulses.
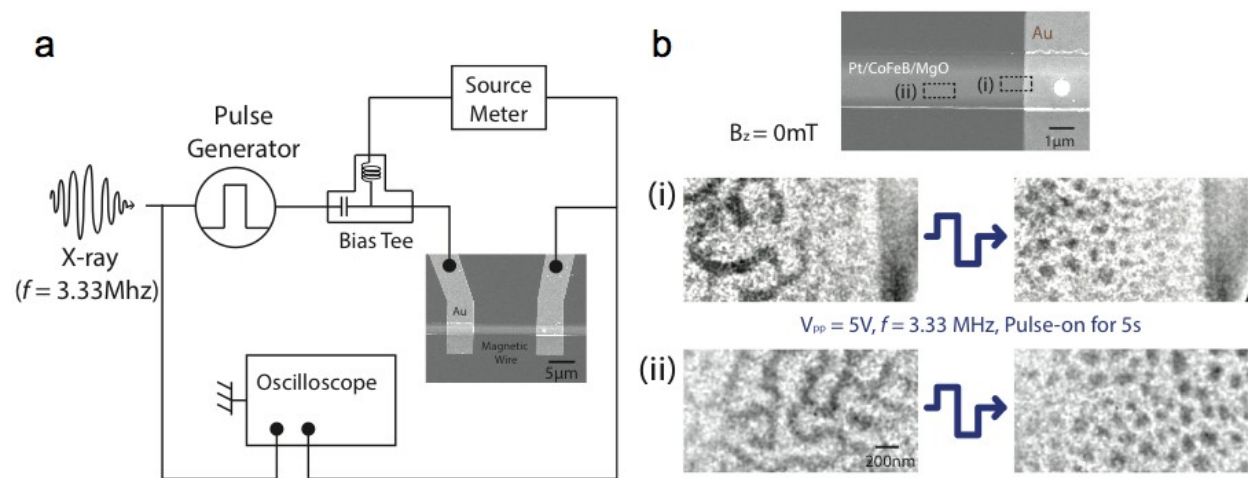
Figure 4. Micromagnetic simulations on dynamic skyrmions triggered by spin orbit torques. a. Top-view of a simulated skyrmion structure at its equilibrium state when B_z=48 mT. **b.** Pulse profile used for the simulation, which is slightly different from the actual profile that was influenced by impedance mismatching. **c.** Time-dependent skyrmion size variation when we considered (i) SOT-only, (ii) Oersted field-only and (iii) SOT and Oersted field models, respectively. **d.** Experimentally measured (left-axis) and computed (right-axis) skyrmion diameter as a function of pulse delay time. **e.** Time-dependent skyrmion travel distance with (i) SOT-only, (ii) Oersted field-only and (iii) SOT and Oersted field models, respectively. **f.**

Experimentally measured (left-axis) and computed (right-axis) skyrmion travel distance as a function of pulse delay time. Note that y-axis scales are different between the experiment and computational model in **d** and **e.**
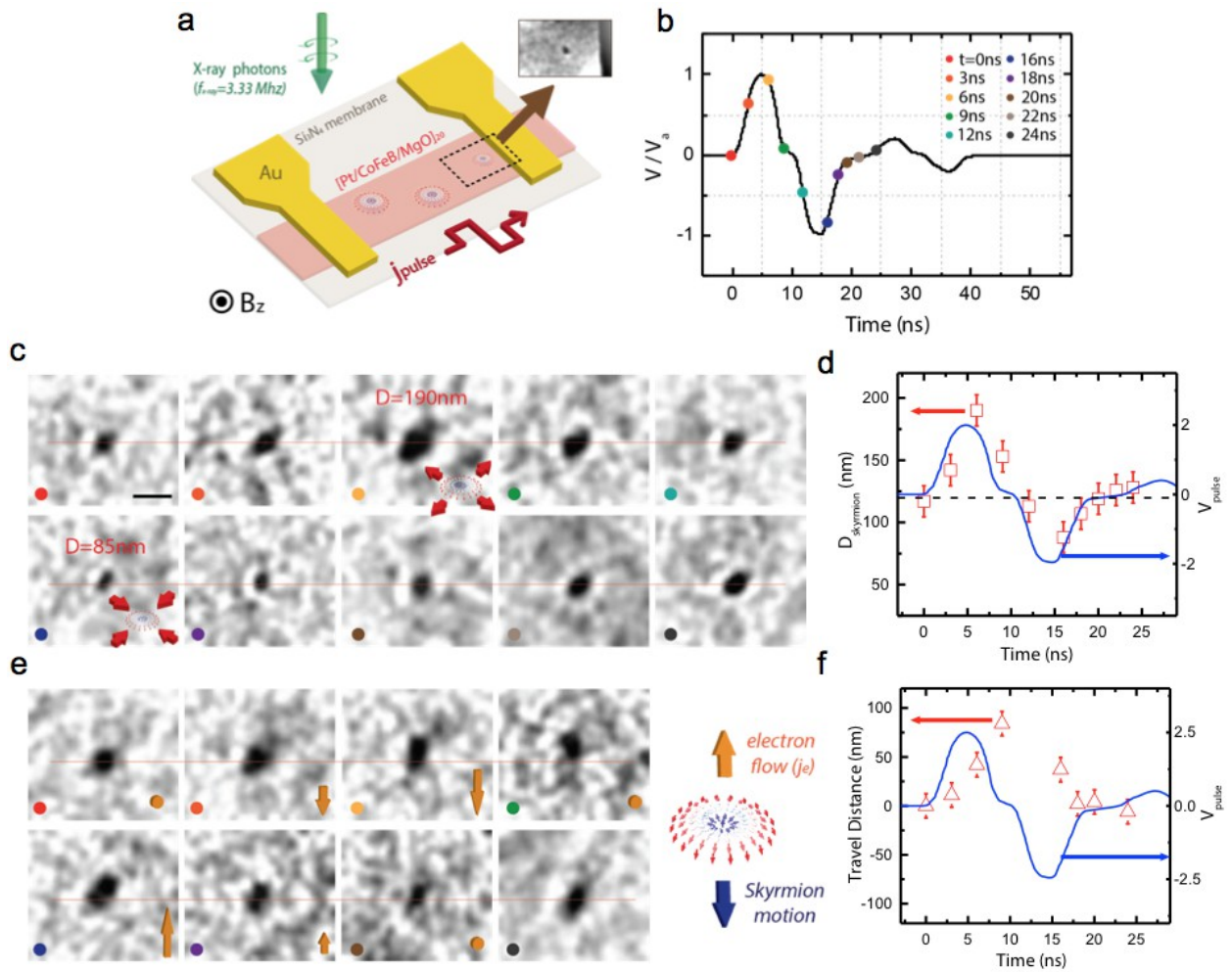
Figure 5. Micromagnetic simulations on inertial motion of a skyrmion and its deformation. **a.** Time-dependent pulse profile and skyrmion travel distance acquired from Fig. 4b and 4d. **b.** First time-derivitive of Fig. 5a, showing the velocity and pulse amplitude as a function of pulse delay time.
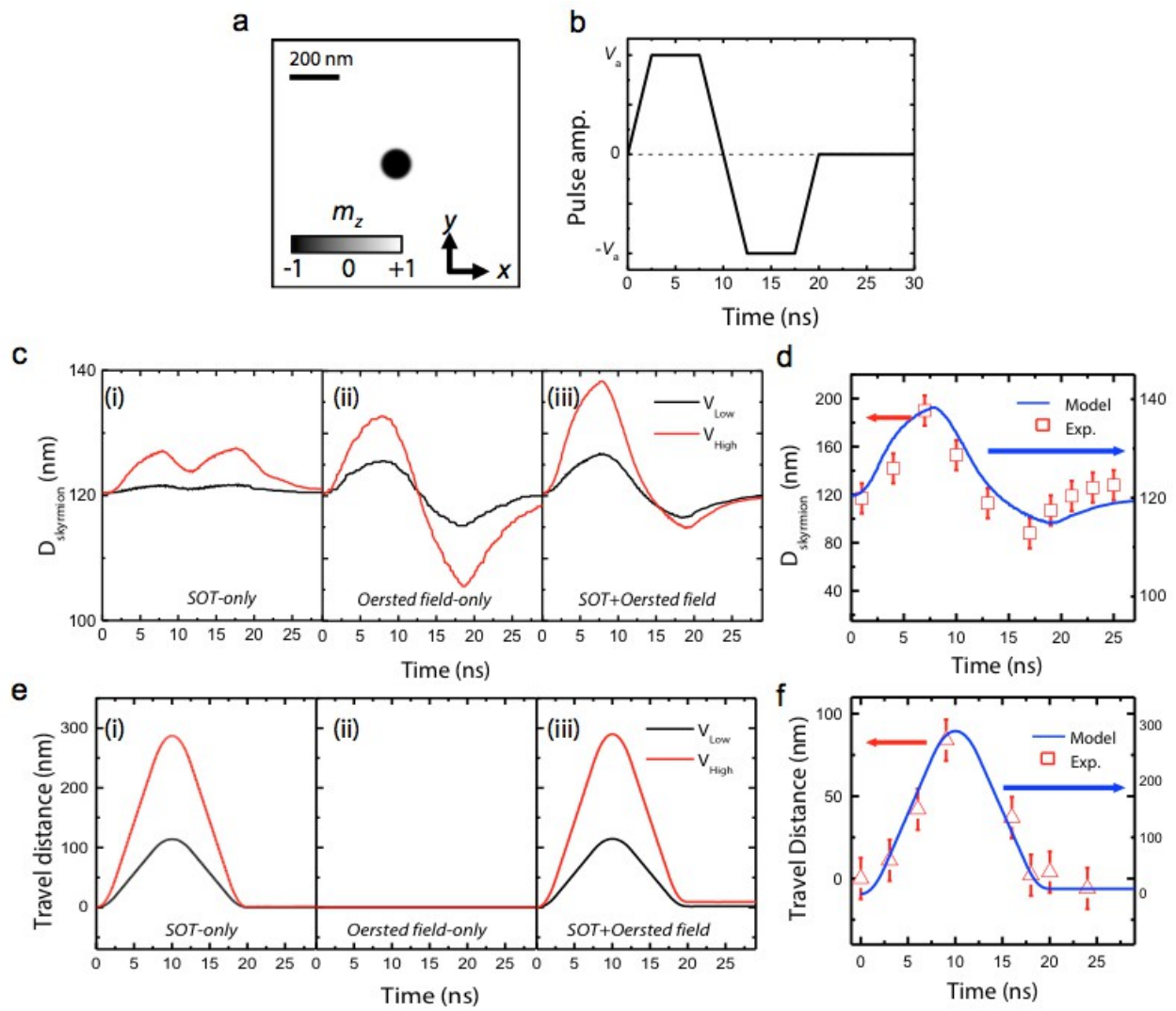
Figure 1

a

Pulse Generator

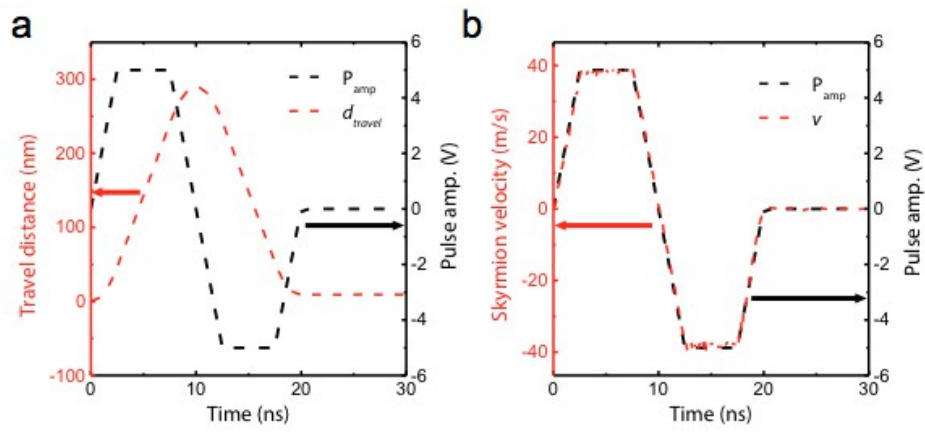Source Meter

X-ray (f = 3.33Mhz)

Bias Tee

Oscilloscope

Au

Magnetic Wire

5μm

b

Au

Pt/CoFeB/MgO

(ii)   (i)

B_z = 0mT

1μm

(i)

V_{pp} = 5V, f = 3.33 MHz, Pulse-on for 5s

(ii)

200nm

Figure 2

Figure 3

Figure 4

Figure 5